Catalytic decomposition of biogas to produce H_2-rich fuel gas and carbon nanofibers. Parametric study and characterization.

S. de Llobet[a], J.L. Pinilla[a], M.J. Lázaro[a], R. Moliner[a] , I. Suelves[a*]

[a]*Instituto de Carboquímica. CSIC. C/ Miguel Luesma 4. 50018 Zaragoza, Spain*

Abstract

One of the main problems that our society must deal with in a near future is the progressive substitution of traditional fossil fuels by different energy sources, such as renewable energies. In this context, biogas will play a vital role in the future. Nowadays, one of the most important uses of biogas is the production of heat and electricity from its direct combustion in co-generation plants. An interesting alternative consists on its direct valorisation to produce a syn-gas that can be further processed to produce chemicals, liquid fuels, or hydrogen. Results showed in this work evidenced that catalytic decomposition of biogas (CH_4/CO_2 mixtures) can be carried out with a Ni/Al_2O_3 catalyst obtaining simultaneously a syn-gas with high H_2 content together with carbonaceous nanostructured materials with high added value. The parametric study revealed that temperature, WHSV (Weight Hourly Space Velocity, defined here as the total flow rate at normal conditions per gram of catalyst initially loaded) and CH_4:CO_2 feed ratio influence directly in CH_4 and CO_2 conversion, H_2:CO ratio and carbon generation (gC/g_{cat}). It was also evidenced that carbon structure depends on temperature. At 600ºC, fishbone like nanofibers with no hollow core are obtained while at 700ºC a mixture of fishbone and ribbon like nanofibers with a clear hollow core are formed.

[*] *Corresponding author: fax: +34 976 73 3318, e-mail address: isuelves@icb.csic.es (I. Suelves)*

1. Introduction

One of the main problems that our society must deal with in a near future is the progressive substitution of traditional fossil fuels by different energy sources, such as renewable energies. The current energetic system based on fossil fuels could no longer be sustained as long as fossil fuels are a finite energetic resource [1]. In addition, the use of such fuels generates problems that are increasingly important. Among them, global warming caused by increasing emissions of greenhouse gases (GHG) into the atmosphere is one of the most important [2]. Unfortunately, the complete replacement of fossil fuels by other energy sources, as renewable, is currently unfeasible [3] and a gradual replacement that can last decades is expected to occur.

In this context, biogas from wastes, residues, and energy crops will play a vital role in future [4]. Biogas is a versatile renewable energy source, composed mainly of CH_4 and CO_2 [5] although it contains also traces of other gases such as N_2, H_2, H_2S, Ar, or CO [6]. In 2009, European primary energy production from biogas rose to 8.3 million tons of oil equivalents (Mtoe) with a yearly increase of more than 4.3% [7].

Nowadays, one of the most important uses of biogas is the production of heat and electricity from its direct combustion in co-generation plants. An interesting alternative consists on its direct valorisation by means of reacting the main components of the biogas composition, i.e. CH_4 and CO_2 -the so-called dry reforming of methane- to produce a syn-gas that can be further processed to produce chemicals, liquid fuels, or hydrogen. In the latter case, due to the renewable character of biogas, the process can be classified as CO_2 neutral hydrogen production. However, one of the most important challenges that practical implementation of dry reforming has to address is the

deactivation of the catalysts due to carbon formation [8]. This issue is even of more significance for the case of biogas mixtures, since the higher CH_4/CO_2 ratio eventually provokes larger amount of carbon depositions that rapidly deactivate the catalysts. To avoid carbon formation, noble metals (Pd, Rh, Ir, Pt or Ru) have been studied since the carbon formation is greatly inhibited [9]. However, their high cost make them unsuitable for large scale applications and therefore, researchers attention is mainly focused on catalyst based on transition metals such as Ni, Co and Fe [10-12]. In the case of nickel based catalysts, the minimization of carbon deposits is achieved either by using different supports such as Al_2O_3, CaO, La_2O_3 or SiO_2 [13-15], or doping with other elements, such as Mn, K, Sn, Ca [13] or rare earth mixtures [16].

A different approach to overcome the deactivation problems that arose from the carbon formation in reforming of biogas-like mixtures can be carried out attending to the mechanism of the carbon formation itself. The formation of carbon over metal based catalysts in form of tubular nanostructures by the so-called catalytic decomposition of methane (CDM) has been widely studied [17, 18] and the mechanism by which methane is decomposed and carbon appear as long filament is well understood. The mechanism of filamentous carbon formation from methane decomposition over nickel based catalysts is composed of the following elementary steps [19]: (i) CH_4 chemisorption on the leading face of a catalyst particle through progressive breaking of the four C–H bonds, (ii) aggregation of chemisorbed atomic hydrogen into molecules and further emission into gas phase, (iii) diffusion of atomic carbon through catalyst bulk from the leading face to the trailing face being the driving force the pronounced gradient of carbon concentration existing between these faces and finally, (iv) carbon nucleation in the catalyst trailing face to the formation of carbon nanofibers. Catalyst deactivation occurs depending on the relative rates of the different elemental step rates involved in

the process: thus, if methane decomposition rate and thereafter carbon formation rate, are higher than the rate of carbon diffusion through the nickel bulk, then carbon is accumulated onto the leading face of the nickel particle and it finally ends covered by graphitic layers which hinder the methane diffusion to the nickel active sites, leading to catalyst particle deactivation. On the contrary, if carbon formation rate is lower than the carbon diffusion rate, then carbon nanofibers may growth without catalyst deactivation. The achievement of this equilibrium between the different reaction rates involved in the mechanism pathway in which carbon deposition occurs as nanofiber without catalyst deactivation has been proved experimentally using Co-based catalysts in the methane decomposition reaction [20]. Accordingly, in a previous work we showed that co-feeding CO_2 inhibited significantly nickel particle encapsulation when compared to methane decomposition reaction. This phenomenon was attributed to the changes in the relative rates of the aforementioned processes, by reducing the carbon formation rate because of the event of the Boudouard reaction, therefore reducing the amount of carbon accumulated around the nickel particles [21].

Taking this fact into account, we proposed the catalytic decomposition of CH_4:CO_2 mixtures similar to those found in the biogas composition –from now on called Catalytic Decomposition of Biogas (CDB) [21]- for the production of a syn-gas and a solid carbon product in form of high valuable carbon nanostructures avoiding catalyst deactivation. It is interesting noting that these carbonaceous structures have been shown to posses multiple applications such as graphite precursors to be used as anodes in ion lithium batteries [22], catalyst supports [23] or polymer additives [24], among many others.

In an effort to expand our previous work on the CDB, we present a parametric study carried out in a fixed bed reactor using a Ni/Al_2O_3 based catalyst to determine the influence of some operating conditions (temperature, space velocity and CH_4:CO_2 ratios) on the biogas conversion and catalyst deactivation. Finally, the characteristics of the nanostructured carbonaceous material produced, as a function of the operating conditions, are determined from a variety of analysis techniques.

2. Experimental

2.1. Catalysts preparation

A Ni based catalyst using Al_2O_3 as support with a Ni:Al molar ratio of 2:1 previously tested in CDM [25] [26] and CDB [21] - denoted as Ni/Al_2O_3- was prepared by fusion method previously described in [27]: briefly, nitric salt of nickel and aluminium were fused, followed by the decomposition of the mixtures at 350ºC for 1h and calcination at 450ºC for 8h. The powder samples were ground and sieved to obtain a particle size fraction between 100 and 200 μm. The nickel domain size of the calcined fresh catalyst was 19 nm while after the reduction pre-treatment under a H_2 flow was 31 nm [26].

2.2. Experimental procedure

Catalytic experiments were carried out in a fixed-bed quartz reactor, 15 mm i.d, 750 mm height, heated by an electric furnace. Before each activity test, the catalyst was reduced with an H_2 flow at 550ºC for 1h. Three parameters were considered along the study of the CDB: temperature, WHSV (Weight Hourly Space Velocity, defined here as the total flow rate at normal conditions per gram of catalyst initially loaded) and CH_4:CO_2 ratio. To determine the effect of the temperature, three different conditions were studied, namely 600, 650 and 700ºC. For all cases, a flow rate of 100 $mL_N \cdot min^{-1}$ was used and the mass of catalyst loaded in the reactor was modified accordingly (0.2, 0.1 and 0.05 grams, respectively) to obtain a specific WHSV (30, 60 and 120 $L_N \cdot g_{cat}^{-1} \cdot h^{-1}$). CDB experiments were carried out with a gas mixture of CH_4 and CO_2 with different CH_4:CO_2 ratio (1:1, 1.5:1 and 2.33:1). Outlet gas samples were analysed by means of

gas chromatography in a HP 5890 series II equipped with two packed columns (Molecular Sieve and Porapack) and a TCD detector.

2.3. Characterization methods

The textural properties of the samples after reaction were measured by N_2 adsorption at 77 K in a Micromeritics ASAP2020 apparatus. The specific surface areas and pore volumes were calculated by applying the BET method to the respective N_2 adsorption isotherms. X-Ray Diffraction (XRD) patterns were acquired in a Brucker AXS D8 Advance Series 2 diffractometer using a Bragg-Brentano θ–θ configuration, Ni-filtered Cu Kα radiation and a secondary graphite monochromator. The angle range scanned was 3–80º using a counting step of 0.05º and a counting time per step of 3s. The powder XRD patterns were further processed using the accompanying DIFRACplus EVA v8.0 software. Raman spectra of the carbonaceous materials were obtained with a Horiba Jobin Yvon HR800 UV microspectrometer using the green line of an argon laser (λ=532 nm) as an excitation source. Extended scans from 1200 to 1800 cm^{-1} were performed to obtain the first-order Raman spectra of the materials. Samples obtained after CDB experiments were characterized by Transmission Electron Microscopy (TEM) in a JEOL 2010.

3. Results

3.1. Parametric study

3.1.1 Influence of the reaction temperature

In a previous work [21], a thermodynamic study was carried out with a gas mixture mimicking the biogas concentration. This study allowed us to identify the temperature window in which carbon formation is favoured together with high methane

and CO_2 conversions [21]. Accordingly, in this study the effect of the temperature is studied in the range between 600 and 700ºC.

The effect of the temperature on the CH_4 and CO_2 conversions at different WHSV and a CH_4:CO_2 ratio of 1:1 is shown in Table 1. Conversions at equilibrium have been included in brackets to facilitate the discussion. The H_2 concentration on the gas stream leaving the reactor, the H_2:CO ratio, the methane decomposition rate (expressed as milimol of methane reacted per gram of catalyst initially loaded and minute) and the amount of carbon deposited after three hours time on stream are also included in Table 1.

The effect of the temperature on CH_4 and CO_2 conversions is clear. As the temperature is increased, both CH_4 and CO_2 conversions increased. Furthermore, when temperature is increased, both CH_4 and CO_2 conversions are closer to equilibrium and in the case of the CO_2, equilibrium conversions are achieved at 650 and 700ºC (at 30 and 60 $L_N \cdot g_{cat}^{-1} \cdot h^{-1}$). Many reactions are involved in the CDB, but the most important (reaction 1, 2 and 3) are endothermic and so the process is favoured at higher temperatures.

- *Dry reforming:* $CH_4 + CO_2 \leftrightarrow 2\ CO + 2\ H_2$; ($\Delta H^o$=247 kJ·mol^{-1}) (1)

- *Methane decomposition:* $CH_4 \leftrightarrow C + 2\ H_2$; ($\Delta H^o$= 75 kJ·mol^{-1}) (2)

- *Reverse Boudouard reaction:* $C + CO_2 \leftrightarrow 2\ CO$; ($\Delta H^o$= 171 kJ·mol^{-1}) (3)

- *Steam reforming:* $CH_4 + H_2O \leftrightarrow 3\ H_2 + CO$; ($\Delta H^o$= 206 kJ·mol^{-1}) (4)

- *Reverse Water Gas Shift:* $CO_2 + H_2 \leftrightarrow CO + H_2O$; ($\Delta H^o$= 42 kJ·mol^{-1}) (5)

- *Carbon gasification:* $H_2O + C \leftrightarrow CO + H_2$; ($\Delta H^o$=131 kJ·mol^{-1} (6)

- *Methanation reaction:* $CO_2 + 4\ H_2 \leftrightarrow CH_4 + 2\ H_2O$; ($\Delta H^o$= -165 kJ·mol^{-1}) (7)

H_2 and CO concentration are related with CH_4 and CO_2 conversions. H_2 formation depends strongly on methane decomposition reaction (reaction 2). As the temperature is

increased, CH_4 decomposition reaction is favoured and consequently, the H_2 generation. CO formation presents the same behaviour as H_2, but in CO case the reaction involved is the reverse Boudouard reaction (reaction 3). As the temperature is increased (650 and 700ºC), an increment in the CH_4 and CO_2 conversions is observed and therefore, the H_2 and CO concentrations are higher than at 600ºC. It is noted, that for the temperature range studied the CO concentration is higher than the H_2 concentration, and as a result the H_2:CO ratio is lower than one, excepting at 600ºC and 30 $L_N \cdot g_{cat}^{-1} \cdot h^{-1}$. This results agree with a study carry out by Bradford and Vannice [28], which revealed that the apparent activation energy barrier for H_2 formation is higher than CO one. It can also be observed in Table 1, that H_2:CO ratio values are closer to the unity. This ratio permits to employ the syn-gas produced in the Fischer-Tropsch process. Usually, a H_2:CO ratio of two is necessary for this application and when ratios below this value are used a water gas shift unit is required. However, when Fe catalysts are used, the enhancement of the H_2:CO ratio could take place in the Fischer-Tropsch reactor due to its high activity in the WGS reaction and so an extra unit can be avoided [29].

According to kinetics, an increase of the reaction rate coefficient is expected when temperature is increased. Thus the higher the temperature is, the higher the CH_4 decomposition rate becomes as it is observed in Table 1 for the range of temperature studied.

Carbon generation depends strongly on temperature. On the one hand and according to thermodynamics, the amount of carbon deposited decreases when temperature is increased in the range between 600 and 700ºC for a CH_4:CO_2 ratio of 1:1 [30, 31]. Reactions 2, 3 and 6 are all of them favoured at higher temperatures. In the reaction 2, carbon is a product, while in reaction 3 and 6, it acts as a reactant. Therefore, carbon behaviour with temperature is not obvious. Haghighi et al. [32] presented the

standard Gibbs free energy changes of reactions involved in dry reforming of CH_4 as a function of temperature. At 600ºC and according to Gibbs free energy values, the three reactions (reaction 2, 3 and 6) are favoured in order to produce carbon. At 700ºC the trend is reversed and only reaction 2 is favoured in order to produce carbon while reaction 3 and 6 are favoured in the sense of consuming carbon, thus explaining that carbon formation is thermodynamically favoured at lower temperatures.

On the other hand and attending to kinetics, carbon generation is favoured at higher temperatures due to the enhancement of the CH_4 decomposition reaction. In Table 1, experimental values of the carbon deposited per gram of catalyst loaded (gC/g_{cat}) are shown. It is observed that at 700ºC the amount of carbon deposited is lower than at 600ºC for all the space velocities studied. However, at 650ºC, the amount of carbon obtained is higher than at 600ºC. At this point and since carbon deposition values are compared after three hours time on stream, a third aspect, namely deactivation phenomenon, has to be taken into account. At 600ºC, carbon formation is more favoured thermodynamically that at 650ºC, but kinetically, carbon generation is favoured at higher temperatures. At 700ºC, deactivation phenomenon start to be significant, as reflected by the double asterisk located above the values and after a certain time on stream, CH_4 conversion decreases and therefore carbon formation is slightly lower.

As mentioned previously, carbon formation encapsulates catalyst particles causing deactivation. However, depending on the operating conditions it is possible to maintain catalyst stability as it is shown in Figure 1. CH_4 and CO_2 conversions are represented as a function of the temperature and the time on stream for a CH_4:CO_2 ratio of 1:1 and 60 $L_N \cdot g_{cat}^{-1} \cdot h^{-1}$. It is observed that CH_4 and CO_2 conversions remain constant after 180 minutes and at 700ºC, both CH_4 and CO_2 conversions exceeding 70%.

3.1.2 Influence of space velocity

As occurred with the temperature in the previous section, the effect of the WHSV on the CH_4 and CO_2 conversions, the H_2 concentration on the gas stream leaving the reactor, the H_2:CO ratio, the methane decomposition rate and the amount of carbon deposited after three hours time on stream is shown in Table 1.

As expected, the lower the WHSV, the higher the conversions achieved. When a high WHSV is selected, the contact time between reactant gases and the catalyst is reduced and therefore CH_4 and CO_2 conversions diminish. This behaviour is also observed in Figure 2, where the evolution of the CH_4 and CO_2 conversions with time is shown for tests carried out at 650ºC with a molar ratio CH_4:CO_2 equal to 1:1. Significant differences are observed when space velocity is reduced from 120 to 60 $L_N \cdot g_{cat}^{-1} \cdot h^{-1}$. This differences are smaller when space velocity is reduced from 60 to 30 $L_N \cdot g_{cat}^{-1} \cdot h^{-1}$ and in some cases, for example at 650 and 700ºC, inexistent.

The effect of the WHSV on the ratio H_2:CO could be found in Table 1. It is observed that an increase in the WHSV provokes a decrease on the H_2:CO ratio, except for the tests performed at 600°C in which this trend was not observed . It is reported [33] [34], that high WHSV favoured the reverse water gas shift reaction ($CO_2 + H_2 \leftrightarrow CO + H_2O$) and thus diminishes the H_2:CO ratio. Increasing WHSV provokes a decrease on the CH_4 and CO_2 conversions as explained before. As a result, more CO_2 is available to react with H_2 in the reverse water gas shift reaction, diminishing the H_2 concentration and increasing the presence of CO.

Another aspect related with WHSV is the deactivation of the catalyst. No deactivation is observed at 30 or 60 $L_N \cdot g_{cat}^{-1} \cdot h^{-1}$, whereas at 120 $L_N \cdot g_{cat}^{-1} \cdot h^{-1}$, a decrease in CH_4 conversion after 1 hour time on stream (Figure 2) reveals that the catalyst is

being deactivated progressively. The same behaviour is observed for CO_2 conversion. As mentioned in the Introduction section, deactivation phenomenon depends on the relative rates of the different elemental step rates involved in the process. For a given temperature, carbon diffusion rate through the nickel bulk is constant and it does not depend on the WHSV. However, as the WHSV is increased, CH_4 decomposition rate ($mmol \cdot g_{cat}^{-1} \cdot h^{-1}$) and thereafter carbon formation rate are increased. At 30 or 60 $L_N \cdot g_{cat}^{-1} \cdot h^{-1}$ no catalyst deactivation is observed (Figure 2) and therefore CH_4 decomposition rates are lower than carbon diffusion rates. But at 120 $L_N \cdot g_{cat}^{-1} \cdot h^{-1}$, a slight deactivation is observed (Figure 2) and thus CH_4 decomposition rate is expected to be higher than carbon diffusion rate.

3.1.3 Influence of the composition

Since this study is aimed at the hydrogen production from biogas, and since CH_4 and CO_2 fractions in biogas are variables, it is necessary to determine the influence of the composition of biogas in the most important parameters. Table 2 shows the effect of the composition on CH_4 and CO_2 conversions, H_2 concentration, H_2:CO ratio, CH_4 decomposition rate and the amount of carbon deposited after three hours time on stream. The effect of the composition is studied in a range representative of biogas. CH_4:CO_2 ratios equal to 1:1, 1.5:1 and 2.33:1 are chosen to carry out this study. Figure 3 shows the CH_4 conversion as a function of the composition and the time on stream for two different temperatures (600 and 700ºC) and fixing the WHSV (60 $L_N \cdot g_{cat}^{-1} \cdot h^{-1}$). At 700ºC, it is observed that the higher the value of CH_4:CO_2 ratio is, the lower the CH_4 conversion becomes. The higher the CH_4:CO_2 ratio is, the higher the CH_4 concentration in the feed is. Consequently, the quantity of CH_4 that does not react is greater. The same behaviour is observed at 600ºC.

Another variable which is influence by the feed composition is the H_2 concentration on the gas stream leaving the reactor. In Table 2 it is observed that the H_2 concentration increases with the CH_4:CO_2 ratio even if the CH_4 conversion decreases.

Moreover, CH_4:CO_2 ratio influence on the catalyst deactivation rate. At 700ºC, CH_4 conversion for a CH_4:CO_2 ratio of 1:1 remains constant at 73% after three hours on stream (Figure 3). As CH_4:CO_2 ratio is increased (CH_4:CO_2 equal to 1.5:1 and 2.33:1), more quantity of CH_4 is available to react and as a result, carbon formation due to methane decomposition reaction is favoured, causing an encapsulation of the metallic particles and a progressive deactivation of the catalyst. The greater the amount of CH_4 is fed, the more unstable behaviour of the catalyst results and the faster the CH_4 conversion decreases. As it is shown in Table 2, when a CH_4:CO_2 ratio of 1:1 is fed into the reactor at 60 $L_N \cdot g_{cat}^{-1} \cdot h^{-1}$, no clear deactivation is observed in the range of temperature studied. However, when a ratio of 1.5:1 is selected, deactivation phenomenon is clearly observed at 700ºC. Finally, if the ratio is increased until 2.33:1, deactivation is also observed at 650ºC.

It is known that high CH_4:CO_2 ratios (1.5:1 and 2.33:1) favour carbon formation and thus the deactivation of the catalyst is dramatically promoted. However, it is possible to obtain constant CH_4 and CO_2 conversions by varying WHSV and/or temperature. Diminishing temperature 100ºC (from 700 to 600ºC), a stable catalytic behaviour is achieved for mixtures with a CH_4:CO_2 ratio of 1.5:1 and 2.33:1 and at 60 $L_N \cdot g_{cat}^{-1} \cdot h^{-1}$. After three hours on stream, CH_4 conversion at 600ºC for a CH_4:CO_2 ratio of 2.33:1 remains constant over time and in addition, is higher than at 700ºC (35% and 25% respectively) as it is seen in Figure 3. Again, this behaviour is related with CH_4 decomposition rate. When deactivation is observed, CH_4 decomposition rate is higher

than carbon diffusion ones. To reverse this behaviour, temperature could be reduced 50ºC for CH_4:CO_2 ratio of 1.5:1 and 100ºC for a ratio of 2.33:1.

As shown throughout this section, CDB can be carried out avoiding catalyst deactivation by modifying the operation conditions as a function of the feed composition. Since biogas composition cannot be changed without performing a separation step, temperature and WHSV are the most important operation conditions that can be adjust to prevent catalyst deactivation. In Table 3, the most important parameters of the CDB (CH_4 conversion, $\%H_2$, H_2:CO ratio and gC/g_{cat}) are shown at the optimum operation conditions. The criteria selected to determine the optimum operation conditions for the different CH_4:CO_2 ratio studied were: no catalyst deactivation should be observed and the higher CH_4 decomposition rate should be reached. It is observed that CH_4 conversion decreases when the CH_4:CO_2 ratio is increased, and for ratios of 1.5:1 and 2.33:1 conversions are far away from equilibrium. H_2:CO ratios obtained for all the feed composition studied allows to use the syn-gas produced in the Fischer-Tropsch process. At the same time, nanostructured carbonaceous material with a high added value is obtained and the amount deposited increases with the CH_4:CO_2 ratio.

3.2. Characterization of the carbon nanofibers

3.2.1 Structural and textural parameters

Samples obtained after CDB (used catalyst + deposited carbon) presented a graphitic structure as evidenced by the presence of an intense symmetric peak (002) at approximately 26º (XRD patterns not shown). Ni was also observed whereas no presence of NiO was detected, showing that the active phase was completely reduced prior to CDB tests. Crystal domains size (L_c), interlayer spacing (d_{002}), catalyst particle

diameter after reaction (dp), BET surface area (S_{BET}) and I_D/I_G Raman ratio of the carbonaceous samples are shown in Table 4.

Carbons deposited on the catalyst after CDB show a significant degree of structural order as reveal the interlayer spacing (d_{002}) of the analyzed samples. Values in the range of 0.3383-0.3404 nm are obtained. According to Franklin's classification, this range corresponds to a turbostratic carbon structure [35]. Turbostratic carbon is generally regarded as a variant of hexagonal high ordered graphite with higher d_{002} values ($d_{002,\ turbostratic} > d_{002,\ graphite}$), low values of L_c and L_a (crystal domain sizes) and where graphite crystallites have an essentially random orientation. Despite the fact that L_c does not vary considerably, an increase in the L_c is observed when temperature is increased for all the CH_4:CO_2 ratios analyzed. Samples present values between 5.42 and 5.75 nm. In the case of the d_{002} is not possible to determine a relationship between the operation conditions and the graphitization degree, however all the values are close to the graphite interlayer spacing (d_{002}=0,3354 nm), in a narrow range and differences are not significant.

Catalyst particle diameter (dp) was 31 nm before reaction while for spent catalyst was in the range between 34.5-42.3 nm. An increased in the diameter is appreciated. This effect could be explained by the fact that the temperature reached during the reaction (600-700ºC) is higher than in the reduction period (550ºC), inducing a regrouping of the catalyst clusters.

The specific surface area is associated with the presence of several types of mesopores that are located in both the nanofiber interior along the axis and the spaces between the filaments in those areas of granules with varying picking density [36]. S_{BET} samples are shown in Table 4. A decrease is observed when temperature is increased regardless of the CH_4:CO_2 ratio fed. At higher temperatures, carbon nanofibers (CNFs)

acquire a greater graphitic character and consequently a more ordered surface, thus explaining the observed trend. Nevertheless, values are in a narrow range (94-105 m^2/g) and differences are not very large.

Finally, samples were characterized by Raman spectroscopy, after which two well resolved bands were observed: The G (at ~ 1350 nm) and the D (at~ 1580 nm) band. The G band is associated with the in-plane carbon-carbon stretching vibrations of graphite layers, whereas D band is related to graphite imperfections. The intensity ratios of these two bands (I_D/I_G) are exposed in Table 4.

As expected, an increase in the reaction temperature enhances the deposition of more ordered CNFs, as derived from the increase in the crystal domain size (L_c) as well in the reduction of both the S_{BET} and the I_D/I_G ratio.

3.2.2 TEM study

Based on the results shown in Table 4, a slight influence of the temperature in the CNFs properties is observed but no influence of the CH_4:CO_2 ratio or the WHSV are clearly detected. Nevertheless, apparent differences among samples are observed from TEM micrographs. Even though WHSV influence is still no significant, the effect of the temperature or the CH_4:CO_2 ratio is clear.

Figure 4 shows some representative micrographs obtained of the samples after CDB. In Figure 4, temperature effect is appreciated. At 600ºC (Figure 4A and 4B) fishbone like nanofibers, which are characterized by the inclination of the graphene layers with respect to the fibre axis, are formed. On the other hand, a mixture of fishbone and ribbon like nanofibers are formed a 700ºC (Figure 4C). Ribbon structures are straight, unrolled graphene layers that are parallel to the fibril axis with non-cylindrical cross-sections [37]. These carbonaceous structures bear a striking

resemblance with multi-walled carbon nanotubes composed by concentric graphene sheet rolled up into a cylinder with increasing diameter and coaxially disposed, being not possible to differentiate them from the TEM study [37]. However, since the conditions used to obtain the carbonaceous structures shown in Figure 4 differ only in the reaction temperature (600 vs. 700ºC), and taking into account that the TEM picture shown in Figure 4A and 4B is commonly considered as a fishbone (also called herringbone) CNF, it is likely that the carbon deposited at 700ºC may have a similar graphene arrangement to the one obtained at 600ºC. Thus, for the case of the fibre shown in Figure 4C, it seems more plausible the adoption of ribbon like arrangement, so that the main difference as respect to the fibres observed at 600ºC would be the lack of graphene inclination with respect the fibre axis, rather than having a completely new rearrangement in form of concentric graphene sheets rolled up.

The structure of the CNF is related to the catalyst particle shape. At 600ºC (Figure 4B), the trailing face of the particle presents an arrow shape resulting in fishbone nanofibers whose graphene layers acquire the inclination of the catalyst particle. At 700ºC (Figure 4D), catalyst particles present an elongated, poorly defined shape. As a result, both structures could be formed depending on the trailing face of each catalyst particle.

CNFs hollow core also depends on the temperature. At 600ºC, due to the well defined shape of the catalyst, no hollow core is appreciated (Figure 4B), resulting in solid core fishbone nanofibers. On the other hand, a clear hollow core is observed in the CNFs obtained at 700ºC (Figure 4C). The hollow core width is related to the width of the trailing face of the catalyst particle and it may represent a third of the total width of the nanofiber.

Another important issue which is observed in TEM micrographs is catalyst covering/uncovering by encapsulating graphitic layers. This phenomenon depends on both temperature and CH_4 feed concentration. While at 600ºC no covered catalyst particles are observed (Figure 4B), at 700ºC encapsulated catalyst particles are noted (Figure 4D, Figure 5A and B). The degree of covering depends on the CH_4:CO_2 ratio. The higher the CH_4 feed concentration is, the greater the number of encapsulated catalyst particles is. This is in good agreement with the results presented in the parametric study in which a decrease in both CH_4 and CO_2 conversion was observed with time. This decreasing effect was more pronounced when a high CH_4 concentration was fed. This behaviour is related to the net rate of carbon deposition on the leading face of the catalyst particle. The higher the temperature or the CH_4 concentration are, the greater the rate of carbon formation is and consequently the encapsulating degree.

4. Conclusions

Results showed in this work evidenced that catalytic decomposition of biogas (CH_4/CO_2 mixtures) can be carried out with a Ni/Al_2O_3 catalyst obtaining simultaneously a syn-gas with high H_2 content together with carbonaceous nanostructured materials with high added value.

The parametric study revealed that temperature, WHSV and CH_4:CO_2 feed ratio influence directly in CH_4 and CO_2 conversion, H_2:CO ratio and carbon generation (gC/g_{cat}).

A temperature increase provokes CH_4 and CO_2 conversions increase. Furthermore, thermodynamics predicts a decrease of the gC/g_{cat} with temperature. Nevertheless, a valley is observed between 600 and 700ºC. Two opposite effects take place: kinetics and thermodynamics, but a third aspect should be taken into account, catalyst deactivation.

An increase of the WHSV results in a decrease of both CH_4 and CO_2 conversions and the H_2:CO ratio. By increasing the WHSV, the active sites number is decreased and consequently catalytic adsorption reactions are impaired. On the other hand, high WHSV favoured the RWGS reaction and thus diminishes the H_2:CO ratio.

It was observed that catalytic deactivation was related with carbon formation which encapsulates leading face catalyst particle. An increase in the CH_4:CO_2 ratio increases carbon formation as the CH_4 decomposition reaction is favoured. To avoid catalyst deactivation, temperature could be reduced. By diminishing temperature 100ºC, a stable catalytic behaviour is achieved for all the CH4:CO2 ratio analyzed. Moreover,

after three hours on stream, CH4 conversion is higher at 600ºC (35%) than at 700ºC (25%) for a CH_4:CO_2 ratio of 2.33:1.

Carbon structure depends on temperature. At 600ºC, fishbone like nanofibers with no hollow core are obtained while at 700ºC a mixture of fishbone and ribbon like nanofibers with a clear hollow core are formed.

Acknowledgments

The authors acknowledge the Spanish Science and Innovation Ministry for the financial support of the Project ENE2008-06516.

References

[1] Core Writing Team P, R.K and Reisinger, A. (eds.). IPCC, 2007: Climate Change 2007: Synthesis Report. Contribution of Working Groups I, II and III to the Fourth Assessment Report of the Intergovernmental Panel on Climate Change IPCC, Geneva, Switzerland, 104 pp. 2007.

[2] B. Metz ORD, P.R. Bosch, R. Dave, L.A. Meyer (eds). IPCC, 2007: Climate Change 2007: Mitigation. Contribution of Working Group III to the Fourth Assessment Report of the Intergovernmental Panel on Climate Change. 2007.

[3] Zerta M, Schmidt PR, Stiller C, Landinger H. Alternative World Energy Outlook (AWEO) and the role of hydrogen in a changing energy landscape. International Journal of Hydrogen Energy. 2008;33:3021-5.

[4] Weiland P. Biogas production: current state and perspectives. Applied Microbiology and Biotechnology. 2010;85:849-60.

[5] A. Wellinger AL. Biogas Upgrading and utilisation. Task 24: Energy form Biological Conversion of Organic Waste (IEA Bioenergy). 2000.

[6] Huang J, Crookes RJ. Assessment of simulated biogas as a fuel for the spark ignition engine. Fuel. 1998;77:1793-801.

[7] EurObservER. Biogas Barometer. Le journal des énergies renouvelables. 2010;200.

[8] Hu Y, Ruckenstein E. Catalytic Conversion of Methane to Synthesis Gas by Partial Oxidation and CO2 Reforming. Advances in Catalysis. 2004;48:297-345.

[9] Rostrupnielsen JR, Hansen JHB. CO2-Reforming of Methane over Transition Metals. Journal of Catalysis. 1993;144:38-49.

[10] Asai K, Takane K, Nagayasu Y, Iwamoto S, Yagasaki E, Inoue M. Decomposition of methane in the presence of carbon dioxide over Ni catalysts. Chemical Engineering Science. 2008;63:5083-8.

[11] San-José-Alonso D, Juan-Juan J, Illán-Gómez MJ, Román-Martínez MC. Ni, Co and bimetallic Ni–Co catalysts for the dry reforming of methane. Applied Catalysis A: General. 2009;371:54-9.

[12] Murata K, Inaba M, Takahara I, Mimura N. Methane Decomposition over Iron-based Catalysts in the presence of O2 and CO2. Journal of the Japan Petroleum Institute. 2003;46:196-202.

[13] Castro Luna AE, Iriarte ME. Carbon dioxide reforming of methane over a metal modified Ni-Al2O3 catalyst. Applied Catalysis A: General. 2008;343:10-5.

[14] Zhang ZL, Verykios XE. Carbon dioxide reforming of methane to synthesis gas over supported Ni catalysts. Catalysis Today. 1994;21:589-95.

[15] Kroll VCH, Swaan HM, Mirodatos C. Methane Reforming Reaction with Carbon Dioxide Over Ni/SiO2Catalyst: I. Deactivation Studies. Journal of Catalysis. 1996;161:409-22.

[16] Slagtern Å, Olsbye U, Blom R, Dahl IM, Fjellvåg H. Characterization of Ni on La modified Al2O3 catalysts during CO2 reforming of methane. Applied Catalysis A: General. 1997;165:379-90.

[17] Pinilla JL, Moliner R, Suelves I, Lázaro MJ, Echegoyen Y, Palacios JM. Production of hydrogen and carbon nanofibers by thermal decomposition of methane using metal catalysts in a fluidized bed reactor. International Journal of Hydrogen Energy. 2007;32:4821-9.

[18] Pinilla JL, Suelves I, Lázaro MJ, Moliner R, Palacios JM. Parametric study of the decomposition of methane using a NiCu/Al2O3 catalyst in a fluidized bed reactor. International Journal of Hydrogen Energy. 2010;35:9801-9.
[19] Baker RTK, Barber MA, Harris PS, Feates FS, Waite RJ. Nucleation and growth of carbon deposits from the nickel catalyzed decomposition of acetylene. Journal of Catalysis. 1972;26:51-62.
[20] Zhang Y, Smith KJ. CH4 decomposition on Co catalysts: effect of temperature, dispersion, and the presence of H2 or CO in the feed. Catalysis Today. 2002;77:257-68.
[21] Pinilla JL, de Llobet S, Suelves I, Utrilla R, Lázaro MJ, Moliner R. Catalytic decomposition of methane and methane/CO2 mixtures to produce synthesis gas and nanostructured carbonaceous material. Fuel. 2011;90:2245-53.
[22] Garcia AB, Cameán I, Suelves I, Pinilla JL, Lázaro MJ, Palacios JM, et al. The graphitization of carbon nanofibers produced by the catalytic decomposition of natural gas. Carbon. 2009;47:2563-70.
[23] Sebastián D, Calderón JC, González-Expósito JA, Pastor E, Martínez-Huerta MV, Suelves I, et al. Influence of carbon nanofiber properties as electrocatalyst support on the electrochemical performance for PEM fuel cells. International Journal of Hydrogen Energy. 2010;35:9934-42.
[24] Utrilla R, Pinilla JL, Suelves I, Lázaro MJ, Moliner R. Catalytic decomposition of methane for the simultaneous co-production of CO2-free hydrogen and carbon nanofibre based polymers. Fuel. 2011;90:430-2.
[25] Pinilla JL, Utrilla R, Lázaro MJ, Moliner R, Suelves I, García AB. Ni- and Fe-based catalysts for hydrogen and carbon nanofilament production by catalytic decomposition of methane in a rotary bed reactor. Fuel Processing Technology. 2011;92:1480-8.
[26] Pinilla JL, Suelves I, Lázaro MJ, Moliner R, Palacios JM. Influence of nickel crystal domain size on the behaviour of Ni and NiCu catalysts for the methane decomposition reaction. Applied Catalysis A: General. 2009;363:199-207.
[27] Suelves I, Lázaro MJ, Moliner R, Echegoyen Y, Palacios JM. Characterization of NiAl and NiCuAl catalysts prepared by different methods for hydrogen production by thermo catalytic decomposition of methane. Catalysis Today. 2006;116:271-80.
[28] Bradford MCJ, Vannice MA. Catalytic reforming of methane with carbon dioxide over nickel catalysts II. Reaction kinetics. Applied Catalysis A: General. 1996;142:97-122.
[29] Tristantini D, Lögdberg S, Gevert B, Borg Ø, Holmen A. The effect of synthesis gas composition on the Fischer-Tropsch synthesis over Co/[gamma]-Al2O3 and Co-Re/[gamma]-Al2O3 catalysts. Fuel Processing Technology. 2007;88:643-9.
[30] Muradov N, Smith F, Traissi A. Hydrogen production by catalytic processing of renewable methane-rich gases. International Journal of Hydrogen Energy. 2008;33:2023-35.
[31] Li Y, Wang Y, Zhang X, Mi Z. Thermodynamic analysis of autothermal steam and CO2 reforming of methane. International Journal of Hydrogen Energy. 2008;33:2507-14.
[32] Haghighi M, Sun Z-q, Wu J-h, Bromly J, Wee HL, Ng E, et al. On the reaction mechanism of CO2 reforming of methane over a bed of coal char. Proceedings of the Combustion Institute. 2007;31:1983-90.
[33] Yin L, Wang S, Lu H, Ding J, Mostofi R, Hao Z. Simulation of effect of catalyst particle cluster on dry methane reforming in circulating fluidized beds. Chemical Engineering Journal. 2007;131:123-34.

[34] Iwasa N, Takizawa M, Arai M. Preparation and application of nickel-containing smectite-type clay materials for methane reforming with carbon dioxide. Applied Catalysis A: General. 2006;314:32-9.
[35] Franklin R. The structure of graphitic carbons. Acta Crystallographica. 1951;4:253-61.
[36] Fenelonov VB, Derevyankin AY, Okkel LG, Avdeeva LB, Zaikovskii VI, Moroz EM, et al. Structure and texture of filamentous carbons produced by methane decomposition on NI and NI-CU catalysts. Carbon. 1997;35:1129-40.
[37] Martingullon I, Vera J, Conesa J, Gonzalez J, Merino C. Differences between carbon nanofibers produced using Fe and Ni catalysts in a floating catalyst reactor. Carbon. 2006;44:1572-80.

Figure Captions

Figure 1. CH_4 (a) and CO_2 (b) conversions as a function of the temperature and the time on stream. WHSV= 60 $L_N \cdot g_{cat}^{-1} \cdot h^{-1}$ and CH_4:CO_2 ratio of 1:1.

Figure 2. CH_4 (a) and CO_2 (b) conversions as a function of the WHSV and the time on stream. T= 650ºC and CH_4:CO_2 ratio of 1:1.

Figure 3. CH_4 conversion as a function of the time on stream at 600ºC (open symbols) and 700ºC (closed symbols) for different compositions: 1:1 (red line), 1.5:1 (blue line) and 2.33:1 (black line). WHSV = 60 $L_N \cdot g_{cat}^{-1} \cdot h^{-1}$.

Figure 4. TEM micrographs of the carbon nanostructures formed by CDB. "A" and "B": 600ºC, CH_4:CO_2=1:1 and 120 $L_N \cdot g_{cat}^{-1} \cdot h^{-1}$; "C": 700ºC, CH_4:CO_2=1.5:1 and 60 $L_N \cdot g_{cat}^{-1} \cdot h^{-1}$; "D": 700ºC, CH_4:CO_2=1:1 and 120 $L_N \cdot g_{cat}^{-1} \cdot h^{-1}$.

Figure 5. TEM micrographs of the carbon nanostructures formed by CDB. "A": 700ºC, CH_4:CO_2=1.5:1 and 60 $L_N \cdot g_{cat}^{-1} \cdot h^{-1}$; "B": 700ºC, CH_4:CO_2=2.33:1 and 60 $L_N \cdot g_{cat}^{-1} \cdot h^{-1}$.

Table 1. Effect of the temperature and the space velocity ($L_N \cdot g_{cat}^{-1} \cdot h^{-1}$) on CH_4 and CO_2 conversion (conversions at equilibrium have been included in brackets), $\%H_2$, H_2:CO ratio, CH_4 decomposition rate and the amount of carbon deposited per gram of catalyst initially loaded (gC/g_{cat}) at the early stage of the reaction (i.e. 15 minutes). CH_4:CO_2 ratio = 1:1

	CDB with CH_4:CO_2 ratio = 1:1							
Temp. (ºC)	WHSV ($L_N \cdot g_{cat}^{-1} \cdot h^{-1}$)	CH_4 conv.(%)		CO_2 conv.(%)		$\%H_2$	H_2:CO ratio	CH_4 decomposition rate ($mmol \cdot g_{cat}^{-1} \cdot h^{-1}$)	gC/g_{cat} *
600ºC	30	44	[82]	46	[47]	26	0.95	3.59	5.2
	60	44		42		26	0.91	9.72	8.5
	120	34		39		24	0.97	15.24**	10.4
650ºC	30	59	[87]	55	[55]	35	0.97	6.60	5.5
	60	59		55		34	0.94	13.09	9.0
	120	51		52		31	0.87	22.77**	10.4
700ºC	30	73	[91]	67	[67]	42	1.04	8.18	4.6
	60	73		67		40	0.95	16.31	7.0
	120	69		62		35	0.79	30.88**	6.6

*: Carbon deposition after 3 hours time on stream.
**: Deactivation phenomenon is clearly observed.

Table 2. Effect of the feed composition on CH_4 and CO_2 conversion, $\%H_2$, H_2:CO ratio, CH_4 decomposition rate and the amount of carbon deposited per gram of catalyst initially loaded (gC/g_{cat}) at the early stage of the reaction (i.e. 15 minutes).

	WHSV = 60 $L_N \cdot g_{cat}^{-1} \cdot h^{-1}$							
Feed composition	Temp. (ºC)	CH_4 conv. (%)		CO_2 conv. (%)		$\%H_2$	H_2:CO ratio	CH_4 rate ($mmol \cdot g_{cat}^{-1} \cdot h^{-1}$)	gC/g_{cat}*
CH_4:CO_2= 1:1	600ºC	44	[82]	42	[47]	26	0.91	9.72	8.5
	650ºC	59	[87]	55	[55]	34	0.94	13.09	9.0
	700ºC	73	[91]	67	[67]	40	0.95	16.31	7.0
CH_4:CO_2= 1.5:1	600ºC	40	[78]	45	[55]	30	1.26	10.64	12.2
	650ºC	48	[84]	57	[61]	34	1.09	12.74	11.9
	700ºC	65	[89]	72	[72]	46	1.32	17.30**	9.0
CH_4:CO_2= 2.33:1	600ºC	36	[74]	51	[63]	33	1.68	11.40	14.9
	650ºC	47	[81]	66	[69]	43	1.73	14.69**	17.4
	700ºC	58	[87]	77	[78]	49	1.70	18.17**	12.6

*: Carbon deposition after 3 hours time on stream.
**: Deactivation phenomenon is clearly observed.

Table 3. Optimum operation conditions at CH_4:CO_2 ratios studied for the DCB.

Feed composition	Temp (ºC)	WHSV ($L_N \cdot g_{cat}^{-1} \cdot h^{-1}$)	CH_4 conv. (%)	$\%H_2$	H_2:CO ratio	gC/g_{cat} *
CH_4:CO_2= 1:1	700ºC	60	73	40	0.95	7.0
CH_4:CO_2= 1.5:1	650ºC	60	48	34	1.09	11.9
CH_4:CO_2= 2.33:1	600ºC	60	36	33	1.68	14.9

*: After 3 hours on stream

Table 4. Crystal domain size (L_C), interlayer spacing (d_{002}), catalyst particle diameter after reaction (dp), BET surface area (S_{BET}) of the materials (used catalyst + deposited carbon) and Raman (I_D/I_G) ratio of the carbons deposited on the catalyst after CDB. WHSV of 120 $L_N \cdot g_{cat}^{-1} \cdot h^{-1}$ (CH_4:CO_2 ratio 1:1) and 60 $L_N \cdot g_{cat}^{-1} \cdot h^{-1}$ (1.5:1 and 2.33:1).

Feed composition	Temp. (ºC)	L_C (nm)	d_{002} (A)	dp Ni (nm)	S_{BET} (m^2/g)	I_D/I_G
CH_4:CO_2=1:1	600ºC	5.54	0.3393	42	105	1.25
	700ºC	5.75	0.3387	38	94	1.11
CH_4:CO_2=1.5:1	600ºC	5.48	0.3389	40	97	1.23
	700ºC	5.72	0.3404	38	95	0.91
CH_4:CO_2=2.33:1	600ºC	5.54	0.3383	37	100	1.27
	700ºC	5.67	0.3389	34	93	1.26

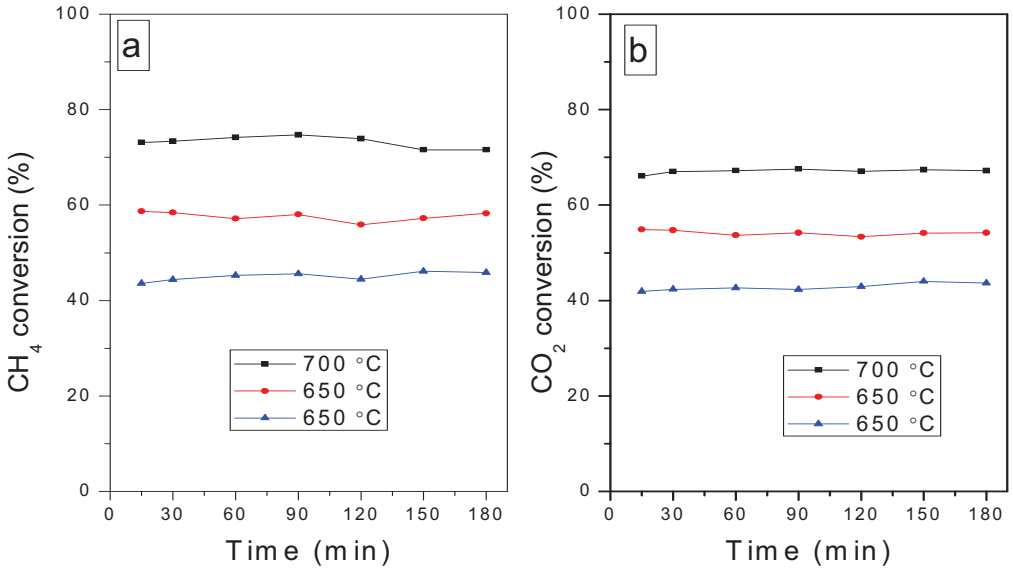

Figure 1. CH_4 (a) and CO_2 (b) conversions as a function of the temperature and the time on stream. WHSV= 60 $L_N \cdot g_{cat}^{-1} \cdot h^{-1}$ and CH_4:CO_2 ratio of 1:1.

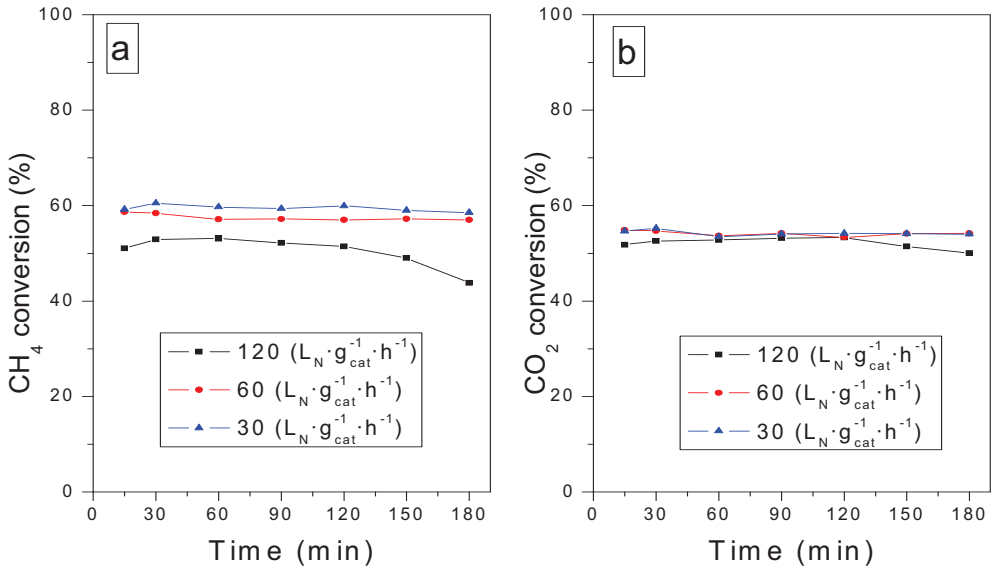

Figure 2. CH_4 (a) and CO_2 (b) conversions as a function of the WHSV and the time on stream. T= 650ºC and CH_4:CO_2 ratio of 1:1.

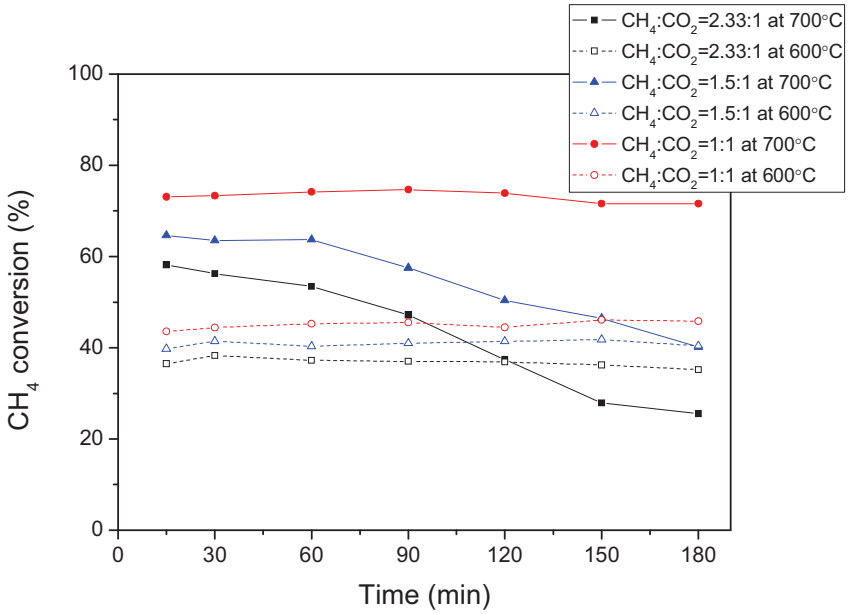

Figure 3. CH_4 conversion as a function of the time on stream at 600ºC (open symbols) and 700ºC (closed symbols) for different compositions: 1:1 (red line), 1.5:1 (blue line) and 2.33:1 (black line). WHSV = 60 $L_N \cdot g_{cat}^{-1} \cdot h^{-1}$.

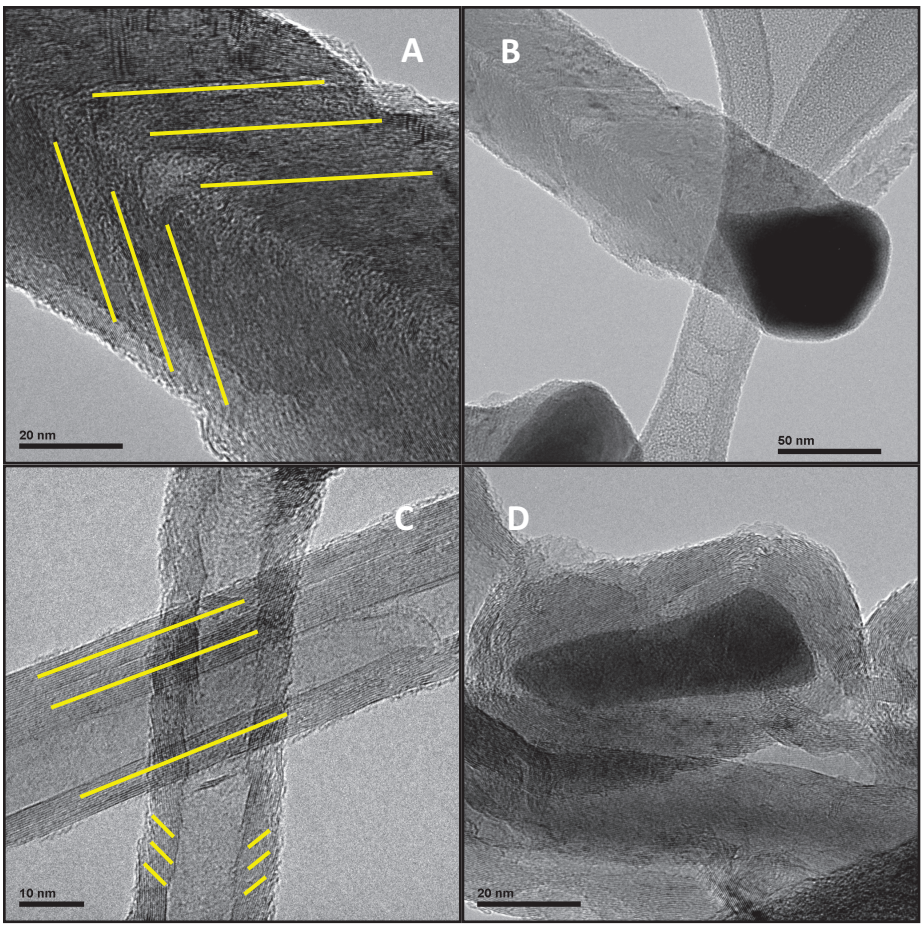

Figure 4. TEM micrographs of the carbon nanostructures formed by CDB. "A" and "B": 600ºC, CH_4:CO_2=1:1 and 120 $L_N \cdot g_{cat}^{-1} \cdot h^{-1}$; "C": 700ºC, CH_4:CO_2=1.5:1 and 60 $L_N \cdot g_{cat}^{-1} \cdot h^{-1}$; "D": 700ºC, CH_4:CO_2=1:1 and 120 $L_N \cdot g_{cat}^{-1} \cdot h^{-1}$.

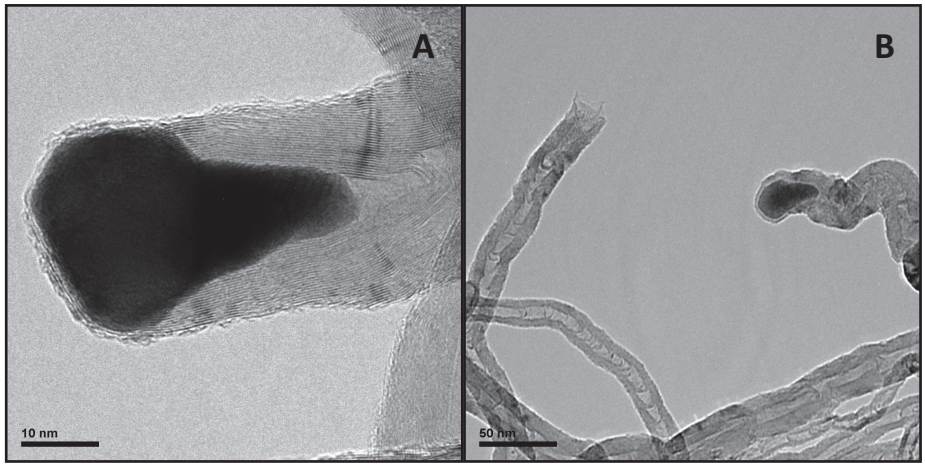

Figure 5. TEM micrographs of the carbon nanostructures formed by CDB. "A": 700ºC, CH_4:CO_2=1.5:1 and 60 $L_N \cdot g_{cat}^{-1} \cdot h^{-1}$; "B": 700ºC, CH_4:CO_2=2.33:1 and 60 $L_N \cdot g_{cat}^{-1} \cdot h^{-1}$.